A molecular dynamics simulation study of elastic properties of HMX

Thomas D. Sewell and Ralph Menikoff
Theoretical Division, Detonation Theory and Application Group, Los Alamos National Laboratory, Los Alamos, New Mexico 87545

Dmitry Bedrov and Grant D. Smith
Department of Materials Science and Engineering and Department of Chemical and Fuels Engineering, University of Utah, Salt Lake City, Utah 84112

(Received 21 April 2003; accepted 17 June 2003)

Atomistic simulations were used to calculate the isothermal elastic properties for β-, α-, and δ-octahydro-1,3,5,7-tetranitro-1,3,5,7-tetrazocine (HMX). The room-temperature isotherm for each polymorph was computed in the pressure interval $0 \leqslant p \leqslant 10.6$ GPa and was used to extract the initial isothermal bulk modulus K_o and its pressure derivative using equations of state employed previously in experimental studies of the β-HMX isotherm. The complete elastic tensor for each polymorph was calculated at room temperature and atmospheric pressure. For the case of β-HMX, the calculated elastic tensor is compared to one based on a fit to sound speed data yielding reasonably good agreement. The bulk modulus of β-HMX obtained from equation-of-state fits to the room-temperature isotherm agrees well with that determined from the complete elastic tensor and from volume fluctuations at atmospheric pressure. However, the value of K_o obtained from the isotherm is sensitive to choice of equation of state fitting form and to the weighting scheme employed in the fit. Based upon simulation results and reanalysis of experimental data, the commonly accepted value of the initial isothermal bulk modulus for β-HMX should be revised from a value of $\sim 12.4-13.5$ GPa to $\sim 15-16$ GPa. The present report provides the first accurate determination of the elastic tensors and isotropic moduli for α- and δ-HMX. Predicted values of the shear moduli for α- and δ-HMX are more than a factor of 2 smaller than for β-HMX. © *2003 American Institute of Physics.* [DOI: 10.1063/1.1599273]

I. INTRODUCTION

A. Motivation

The high explosive octahydro-1,3,5,7-tetranitro-1,3,5,7-tetrazocine (HMX, Fig. 1) is the energetic material in a number of high performance military explosive and propellant formulations.[1] HMX exhibits three pure crystal polymorphs at ambient pressure denoted β-,[2,3] α-,[4] and δ-HMX[5] and listed in terms of stability with increasing temperature. The elastic response of HMX is a key ingredient in the formulation of a complete HMX equation of state (EOS). Two general experimental approaches have been applied to obtain the single crystal elastic properties of HMX: measurements of the specific volume as a function of pressure along an isotherm[6,7] and determinations of isentropic sound speeds from impulsive stimulated light scattering methods (ISLS).[8] Isotherm data can be used to obtain the initial isothermal bulk modulus K_o and its initial pressure derivative $K_o' = dK/dp|_{p=0}$ via an assumed EOS fitting form. ISLS sound speed measurements provide a more-or-less direct path to the isentropic elastic tensor, from which the isentropic bulk and shear moduli, as well as other engineering parameters can be extracted. Transformation between isothermal and isentropic parameters is straightforward (Appendix A). Since isotherm data typically correspond to pressures of several or tens of GPa, determination of K_o for comparison to sound speed measurements generally requires extrapolation of the EOS fit to zero pressure, where differences between equations of state are most apparent.

B. Role of simulations

We think that application of molecular simulation tools for the calculation of appropriate thermophysical properties is a viable strategy for obtaining some of the information required as input to mesoscale equations of state.[9] Given a validated potential-energy surface, simulations can serve as a complement to experimental data by extending intervals in pressure and temperature for which information is available. Furthermore, in many cases, simulations provide the only realistic means to obtain key properties, e.g., for explosives that decompose upon melting, measurement of liquid-state properties is extremely difficult, if not impossible, due to fast reaction rates, which nevertheless correspond to time scales that must be resolved in mesoscale simulations of explosive shock initiation.[10] By contrast, molecular dynamics simulations can frequently provide converged values for those properties on time scales below the chemical reaction induction times. Finally, since computational protocols can be designed to mimic experiments, simulations can be used to interpret discrepancies between experimental results, or to determine which among competing analysis methods is most appropriate.

The thermophysical and mechanical properties of HMX

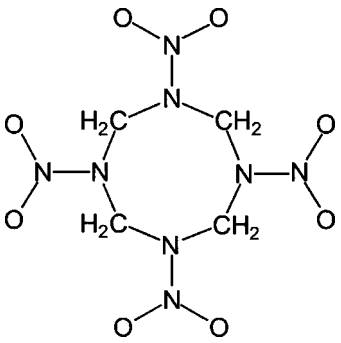

FIG. 1. Chemical structure of HMX

have been the subject of a number of atomistic simulation studies.[11–20] Sewell[12] used a rigid molecule force field, in conjunction with isothermal–isobaric Monte Carlo methods, to compute equilibrium lattice parameters and the room temperature isotherm of β-HMX and RDX. He obtained good agreement with the data of Olinger *et al.*[6] for both materials. Sorescu *et al.* have developed a ''transferable'' intermolecular force field,[21] and have applied it within a rigid-molecule framework to a number of high explosives, including HMX.[13,14] Lewis *et al.*[15] reported quantum chemistry-based predictions of crystal structures, and preliminary values of the bulk modulus, for all three HMX polymorphs.

Bedrov *et al.* have reported previously calculations of the structural properties of the three pure crystal polymorphs,[18–20] and the temperature dependent shear viscosity[16] and thermal conductivity[17] of the liquid phase. The calculations were performed using atomistic molecular dynamics methods with a fully flexible, quantum chemistry-based forcefield, for which particular attention was given to accurate representation of the torsional degrees of freedom associated with the important molecular conformations to enable study of all three crystal polymorphs with a single parameterization.[22] Good agreement with experiment was obtained for equilibrium lattice parameters, linear and volumetric coefficients of thermal expansion, and heats of sublimation ΔH_s for each polymorph.[18,19] It was found that inclusion of intramolecular flexibility is required to obtain the correct ordering of ΔH_s among the three polymorphs.[18] The predicted melt thermal conductivity is consistent with data for the solid state at elevated temperatures.[17]

C. Goals of the present study

The focus of the present work is determination of linear elastic properties of HMX polymorphs at room temperature and atmospheric pressure. For this purpose, molecular simulations of all three polymorphs have been conducted using our validated quantum chemistry-based potential.[22] In particular, we calculate the room-temperature isotherm for each polymorph and extract the bulk modulus and its pressure derivative using commonly employed equation of state fitting forms. In the case of β-HMX, we compare our results to experiment and to other simulations. We apply formalism due to Rahman and Parrinello[23] to compute directly the second-order elastic tensor at room temperature and pressure. We also compute the bulk modulus directly from volume fluctuations. Beyond providing properties that are key elements in the description of the elastic response of HMX, we investigate (1) the level of internal consistency between values of the bulk modulus calculated directly from the elastic tensor and volume fluctuations to values obtained from the equation of state fitting forms, (2) the sensitivity of the latter to the form chosen and the details of how the fit is performed, and (3) the agreement between predicted results and the available experimental data.

II. COMPUTATIONAL DETAILS

The present molecular simulation studies were performed in the isothermal–isobaric (NpT) statistical ensemble.[24] Periodic boundary conditions corresponding to a triclinic primary cell were used. The simulations were performed using the same force field[22] as in our previous studies of HMX.[16–20] We note that our simulations include all degrees of freedom other than covalent bond stretching motions, which were constrained to equilibrium values using the SHAKE algorithm.[24]

The β-, α-, and δ-phases of HMX are monoclinic[2,3] ($P2_1/c$ or, equivalently, $P2_1/n$ space group, $Z=2$ molecules per unit cell, symmetry axis$=b$; 13 independent elastic coefficients[25]), orthorhombic[4] ($Fdd2$, $Z=8$; 9 independent elastic coefficients), and hexagonal[5] ($P6_1$, $Z=6$, symmetry axis$=c$; 5 independent elastic coefficients), respectively. Primary simulation cells containing 96 molecules were used for β-HMX and δ-HMX, corresponding to 48 ($4\times3\times4$) and 16 ($4\times4\times1$) unit cells, respectively. Primary cells containing 64 molecules were used for α-HMX, corresponding to 8 ($2\times1\times4$) unit cells. Electrostatic interactions were treated using the standard Ewald summation.[24] Nonbonded interactions were truncated at 9 Å, 10 Å, and 10 Å for β-, α-, and δ-HMX, respectively. A fixed time step size of one fs was used in all cases. Equilibration runs of one ns duration were performed, followed by production runs of 10 ns and 2 ns for $p=1$ atm and $p>1$ atm, respectively, during which data were collected for subsequent analysis. All of the calculations were performed at 295 K, with a thermostat coupling parameter of 0.01 fs^{-1}.

Our initial approach, published in conference and workshop proceedings,[18–20] was to perform all simulations using the Rahman–Parrinello isothermal–isobaric approach to molecular dynamics (MD),[26] as described by Martyna *et al.*,[27] in which lattice degrees of freedom for the primary cell are explicitly coupled to an external barostat via the stress tensor. However, this requires specification of a parameter corresponding to the strength of coupling to the barostat. We noted in the conference proceedings of Ref. 20 that, while the mean values of the lattice parameters were independent of the specific value chosen for this parameter, higher moments of the distributions did vary with the barostat coupling, at least for the 2–5 ns simulation times considered in our preliminary studies. This sensitivity is troublesome for our purposes, since calculation of the elastic tensor is based on a fluctuation analysis of the microscopic strain tensor. While the results may become independent of the barostat parameter chosen for sufficiently long simulations, it was not practical for us to perform a careful study of this behavior

given the anticipated computational expense. Therefore, in the present study, which should be viewed as superseding the relevant sections of the conference and workshop proceedings, we employed an approach in which isothermal–isochoric (NVT) molecular dynamics of the simulation cell contents was interspersed with isothermal–isobaric (NpT) Monte Carlo (MC) variations of the cell shape and volume. This is valid based on the parametric separability of the partition function in the isothermal–isobaric ensemble,[28]

$$Z_{NpT} = \int_V dV \exp(-\beta pV) \int dq \exp[-\beta E(q;V)]$$

$$= \int_V dV \exp(-\beta pV) Q_{NVT}, \tag{1}$$

where $\beta = 1/\kappa T$ and Q_{NVT} is the partition function in the NVT ensemble.

We used NVT MD to sample the contents of the simulation cell, and an NpT MC algorithm to vary its shape and volume. The latter moves were carried out within a rigid-molecule framework as described previously,[12] using the atomic positions at the end of the preceding flexible molecule NVT MD segment. In practice, 1 ps of NVT MD simulation was followed by a sequence of 100 NpT MC steps. The Monte Carlo step size for a given thermodynamic state was adjusted to yield an acceptance probability of 40%–50%.

III. DATA ANALYSIS

A. Isothermal compression

There are two published measurements of the room temperature isotherm for β-HMX: a 1978 study by Olinger, Roof, and Cady,[6] and one in 1999 by Yoo and Cynn.[7] Olinger *et al.* fit the isotherm to an equation of state (EOS),

$$p(V) = \frac{V_0 - V}{[V_0 - s(V_0 - V)]^2} c^2 \tag{2}$$

based on the hugoniot jump conditions,[29]

$$\frac{V}{V_0} = 1 - \frac{U_p}{U_s}, \quad p = p_0 + \rho_0 U_p U_s, \tag{3}$$

where V is specific volume, U_s and U_p are the pseudoshock velocity and pseudoparticle velocity, respectively; ρ is density; and "0" denotes the reference state (atmospheric pressure in the present case). The fitting parameters c and s in Eq. (2) are related to the bulk modulus K_o and its initial pressure derivative K_o' as $K_o = \rho_o c^2$ and $K_o' = 4s - 1$, respectively.

Yoo and Cynn analyzed their data using the third-order Birch–Murnaghan (BM) EOS,[30]

$$p(V) = \tfrac{3}{2} K[\eta^{-7/3} - \eta^{-5/3}][1 + \tfrac{3}{4}(K' - 4)(\eta^{-2/3} - 1)], \tag{4}$$

where $\eta = V/V_0$ is the compression ratio at pressure p. We note that the third-order BM EOS can be written as a linear function in K_o' and $K_o K_o'$ via the transformation,

$$x = [\eta^{-2/3} - 1]^{-1} - 3, \tag{5}$$

$$y = 2p(V)\{3[\eta^{-7/3} - \eta^{-5/3}][\eta^{-2/3} - 1]\}^{-1},$$

for which the slope and intercept are K_o and $3K_o K_o'/4$, respectively. We refer to this form of the BM EOS as BM-linear. In this plane, low-pressure data points are more heavily weighted than high pressure ones.

Menikoff and Sewell[31] reported recently a re-analysis of the Olinger *et al.*[6] and Yoo and Cynn[7] experiments, applying both equations of state [Eqs. (2) and (4)] to both data sets, to determine which data set and fitting form combination is most consistent with the preponderance of other data for HMX and HMX-based plastic-bonded explosives.[32] We applied all three fitting forms [Eqs. (2), (4), and (5)] to isotherms for β-, α-, and δ-HMX obtained from our simulations and to the two simulation β-HMX isotherms extracted from Fig. 3(b) of Sorescu *et al.* (Ref. 14). We also fit the two experimental β-HMX isotherms to Eq. (5), since this was not included in the work of Menikoff and Sewell.

B. Elastic tensor, volume fluctuations, and isotropic moduli

Published information about the elastic tensor for β-HMX is limited to a partial determination due to Zaug,[8] based on a fit to isentropic sound speeds obtained from impulsive stimulated light scattering (ISLS) measurements at two temperatures. With only two experimental samples of similar orientations available, however, only five of the thirteen nonzero elastic constants could be accurately determined (C_{11}, C_{15}, C_{33}, C_{35}, and C_{55}). To determine a complete set of elastic coefficients corresponding to a globally optimized fit would require additional measurements for different crystal orientations. Zaug used only quasilongitudinal sound speeds in his fitting procedure, due to low signal to noise in the quasitransverse modes and ambiguity in distinguishing between them in his data. We note that the fitted values of the elastic coefficients were adjusted to yield agreement with isentropic sound speeds, but were normalized using the isothermal bulk modulus $K_o = 12.5$ GPa reported in a conference proceeding by Yoo and Cynn,[33] which would appear to be too small based on the analysis due to Menikoff and Sewell.[31]

Rahman and Parrinello[23] showed that the fourth-rank elastic tensor for an anisotropic crystalline solid can be calculated using fluctuations of the microscopic strain tensor,

$$\bar{\bar{S}}_{ijkl} = \frac{\langle V \rangle}{\kappa T} \langle \bar{\varepsilon}_{ij} \bar{\varepsilon}_{kl} \rangle, \tag{6}$$

where $\bar{\bar{S}}_{ijkl}$ and $\bar{\varepsilon}_{ij}$ are elements of the compliance tensor and strain tensor, respectively, and $\langle V \rangle$ is the average volume at a given temperature T (and, implicitly, pressure p). Equation (6) is readily constructed from a suitably large set of observations from an isothermal–isobaric simulation. The fourth-rank elastic tensor can be contracted to second-rank form using Voigt notation and, following the treatment described by Tsai,[34] the stiffness tensor $\bar{C}$ is simply the matrix inverse of the compliance $\bar{S}$ (see Appendix B). The particular form expected for $\bar{C}$ is determined by the symmetry class for a given crystal (e.g., monoclinic, orthorhombic, and hexagonal for β-, α-, and δ-HMX, respectively), and can be used as

TABLE I. Equilibrium lattice parameters and molecular volumes for HMX polymorphs.

Polymorph		a (Å)	b (Å)	c (Å)	α (deg)	α (deg)	γ (deg)	V (Å^3)
β	Sim.[a]	6.531	10.521	7.634	90.00	98.84	90.00	259.18
	Expt.[b]	6.5347	11.0296	7.3549	90	102.69	90	258.6
α	Sim.[a]	14.995	23.975	6.058	90.0	90.0	90.0	272.16
	Expt.[c]	15.14	23.89	5.913	90	90	90	267.3
δ	Sim.[a]	7.62	7.61	33.57	89.99	90.01	120.0	281.17
	Expt.[d]	7.711	7.711	32.553	90	90	120	279.4

[a]Uncertainties are ± 2 or smaller for the last digit given.
[b]Reference 3.
[c]Reference 4.
[d]Reference 5.

a partial check for convergence of the simulation results. Henceforth in the main text and Table III we use Voigt (second-rank) notation exclusively, and therefore use C_{ij} rather than the slightly more cumbersome $\overline{C_{ij}}$.

Given the elastic tensor and Voigt notation definitions given in Eq. (B4), we can obtain Reuss average, isotropic bulk and shear moduli,

$$K_R^{-1}=[S_{11}+S_{22}+S_{33}+2(S_{12}+S_{13}+S_{23})],$$
$$G_R^{-1}=\tfrac{4}{15}[S_{11}+S_{22}+S_{33}-(S_{12}+S_{13}+S_{23}) + \tfrac{3}{4}(S_{44}+S_{55}+S_{66})], \quad (7)$$

corresponding to conditions of uniform stress (the appropriate choice for comparison to isotherm data). The bulk modulus can also be expressed directly from the volume fluctuations,

$$K_V=\frac{\langle V\rangle \kappa T}{\sigma_V^2}, \quad (8)$$

where σ_V is the variance of the volume distribution corresponding to a given pressure and temperature obtained directly from simulations. Volume distributions for all three polymorphs were described accurately by Gaussian functions, indicating that finite-size effects on the predicted moduli are small.

IV. RESULTS AND DISCUSSION

A. Equilibrium lattice parameters and molecular volumes

Calculated and measured lattice parameters and molecular volumes at 295 K and one atmosphere obtained from simulation are summarized for each HMX polymorph and compared to experiment in Table I. The experimental determinations for all three polymorphs were made under thermodynamic conditions identical to those of the simulations. The results are for the most part in good agreement with experiment. The maximum error in any single lattice length is 4.6%, for b in β-HMX; presumably this discrepancy could be reduced by empirical adjustment of force field parameters, which were fit to quantum chemical calculations rather than to experimental data. The average error in molecular volume is 0.9%. The small differences between the present predictions and those reported previously[18] are due to the use of slightly different cutoff and Ewald parameters.

B. β-HMX isotherm

The measured β-HMX isotherms and the one calculated in the present work are shown in Fig. 2. The solid line passing through the simulation results is a fit of the third-order BM-linear equation of state using Eq. (5). The agreement between experiment and simulation is reasonably good; at the highest pressure considered here, 10.6 GPa, the percent difference between our compression ratio and the measurements of Yoo and Cynn[7] is 4.6%, with the simulated isotherm being somewhat stiffer than experiment. The discrepancy is much smaller for comparison to the data of Olinger *et al.*[6]

Application of Eq. (3) to the β-HMX isotherm from simulations leads to the U_s-U_p curve shown in Fig. 3, where negative curvature in the simulation results is clearly evident (filled circles). While such behavior would be anomalous for metals, it is actually expected for pressures below about one GPa in the case of polyatomic molecular crystals, due to complicated molecular packings and intramolecular flexibility, and has in fact been reported for the

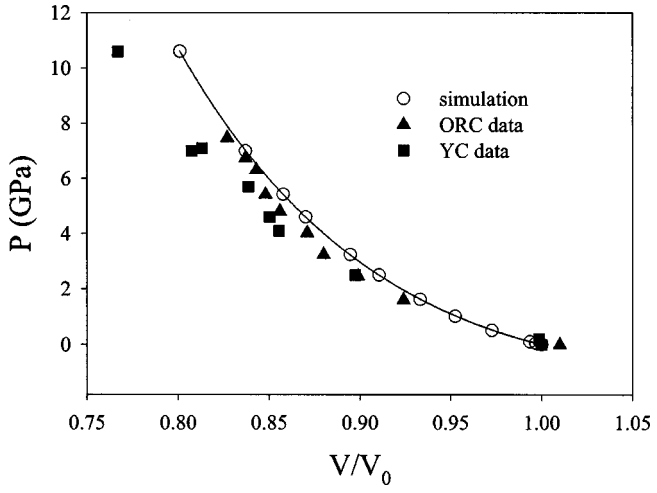

FIG. 2. Isotherms for β-HMX. Open circles: simulation; triangles: Olinger *et al.* (Ref. 6); squares: Yoo and Cynn (Ref. 7). Solid line is the third-order Birch–Murnaghan fit [Eq. (4)] to simulation results, fit via Eq. (5)

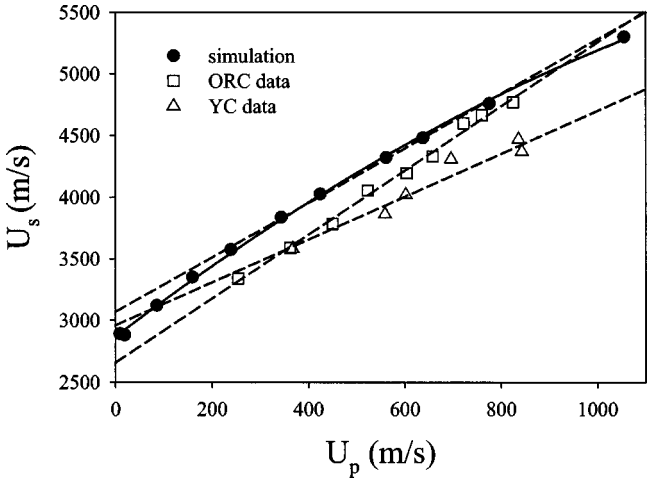

FIG. 3. β-HMX isotherms in the psuedo-(U_s, U_p) plane [Eq. (3)]. Solid line is a quadratic fit to the simulation results. Dashed lines are linear fits to Eq. (3). See text for details.

high explosive pentaerythritol tetranitrate (PETN) where careful studies were performed for low levels of compression.[35] By contrast, the experimental results for β-HMX in the U_s-U_p plane do not exhibit significant curvature due to lack of data at pressures below about one GPa.[36] Thus, estimates of isothermal sound speeds, and hence isothermal bulk moduli, based on extrapolation of these data are likely to be too large. The consequence of employing a linear fit and the lack of low-pressure data on the calculated isothermal bulk modulus can be seen in Fig. 3 by comparing a linear fit ($U_s=c+sU_p$, dashed lines) of the simulation data over the experimental pressure range ($p>1.6$ GPa) to a quadratic fit ($U_s=c+sU_p+tU_p^2$, solid line) of the same data over the entire pressure range. The $U_p=0$ intercepts, which yield c and hence the initial isothermal bulk modulus ($K_o=\rho_o c^2$), differ considerably between the two fits. Hence, the details are important when the goal is to make comparison to ambient sound speed data.

C. Bulk moduli and pressure derivatives

Results for the bulk modulus and its pressure derivative for all three HMX polymorphs are summarized in Table II. For all data sets, we include fits to the U_s-U_p form [Eq. (2)] and both weighting schemes for the third-order Birch–Murnaghan equation of state [Eqs. (4) and (5)]. In the case of the experimental data, values for the moduli based on Eqs. (2) and (4) were taken from the reanalysis of Menikoff and Sewell.[31] Two sets of results are included in the case of Yoo and Cynn, since they reported on the basis of shifts in the

TABLE II. Bulk modulus and its pressure derivative for HMX polymorphs.[a]

		β		α		δ	
Source	Method[b]	K_o	K_o'	K_o	K_o'	K_o	K_o'
		Experiment					
Olinger *et al.* (Ref. 6)	BM	8.4	26.2				
	BM-linear	10.6	18.1				
	U_s-U_p	13.4	9.4				
Yoo and Cynn (<12 GPa) (Ref. 7)	BM	16.7	6.8				
	BM-linear	16.0	7.3				
	U_s-U_p	17.2	5.7				
Yoo and Cynn (<27 GPa) (Ref. 7)	BM	14.5	8.7				
	BM-linear	14.7	8.6				
	U_s-U_p	17.5	5.6				
		Simulation					
Sorescu, $P2_1/c$ (Ref. 14)	BM	9.6	22.0				
	BM-linear	10.9	18.4				
	U_s-U_p	12.2	11.8				
Sorescu, $P2_1/n$ (Ref. 14)	BM	11.6	20.9				
	BM-linear	13.4	16.6				
	U_s-U_p	14.8	10.8				
Lewis *et al.* (Ref. 15)	QC	12.5		38.6		48.0	
This work	fluctuations	15.1		14.1		11.8	
	BM	16.3	11.4	15.5	−13.9	14.1	0.4
	BM-linear	15.5	12.1	14.3	14.0	12.0	8.1
	U_s-U_p	15.6	11.0	14.1	16.8	12.3	4.7

[a]K_o in GPa, K_o' is dimensionless.

[b]BM=from Birch–Murnaghan EOS [Eq. (4)]. BM-linear=from Birch–Murnaghan EOS [Eq. (5)]. U_s-U_p=from U_s-U_p EOS [Eq. (2)]. QC=from quantum chemical calculations (Ref. 15). Fluctuations=from equilibrium volume fluctuations [Eq. (8)] or, equivalently, the equilibrium elastic tensor [using Eq. (7)] at atmospheric pressure.

Raman spectra a phase transition with zero volume change at 12 GPa. Simulation results for the isotherm due to Sorescu *et al.*[14] were extracted by hand from Fig. 3(b) of their work. Predictions of the bulk modulus obtained directly from the elastic coefficients using Eq. (7) and from the volume fluctuations using Eq. (8) were equal to within error bars; thus, only a single value is included.

A few general observations are in order. First, tabulated values of the initial bulk modulus vary by almost a factor of 2, from 8.4 to 17.5 GPa, while values of the pressure derivative vary by almost a factor of 5; even within a given data set, there is significant scatter in these parameters. In practice, the fits are most sensitive at ambient conditions; for high pressures, the differences among them are lessened. This underscores the need for high-precision data, with information extending down to low pressures if the objective is accurate predictions of the initial bulk modulus.

Among the experimental sets, the Yoo and Cynn[7] isotherm leads to more consistent predictions for both K_o and K_o'. Menikoff and Sewell[31] provided a thorough discussion of the two experimental isotherms. Although they obtained values of K_o and K_o' that disagreed significantly with those reported by Yoo and Cynn, they found that their data, fit using the third-order Birch–Murnaghan equation of state, leads to better overall agreement with the other HMX data than does the set of Olinger *et al.*[6] In particular, the isotherm of Olinger *et al.* leads to the prediction of a stiffer equation of state than is obtained from shock hugoniot data[37] for pressed HMX, which is aphysical since the shock hugoniot locus should always lie above the isotherm in the (V,p) plane. As our interest is in the initial bulk modulus and pressure derivative, we make our principal comparisons between the Yoo and Cynn results for $p<12$ GPa, for which $16.0\ \text{GPa}<K_o<17.2\ \text{GPa}$ and $5.7<K_o'<7.3$.

Results obtained using the two calculated isotherms of Sorescu *et al.*[14] and from the quantum chemistry-based cold curve calculations of Lewis *et al.*[15] yield predictions of the β-HMX bulk modulus $9.6\ \text{GPa}<K_o<14.8\ \text{GPa}$. These values are generally consistent with values derived from the Olinger *et al.*[6] isotherm, i.e., roughly 3 GPa lower than the Yoo and Cynn results for $p<27$ GPa. An interesting observation is that the isotherms of Sorescu *et al.* are sensitive to whether the $P2_1/c$ or $P2_1/n$ space group setting is chosen, even though the two are formally equivalent. This is apparently due to the use of independent crystal structure determinations for the two space groups,[2,3] with associated small differences in measured molecular geometries, that were used as input to their rigid-molecule simulations. These differences led in turn to slightly different partial atomic charges used in the potential-energy function for the two cases.[38]

Bulk moduli for β-HMX obtained from the present simulations yield moduli consistent with the Yoo and Cynn results, namely, $15.1\ \text{GPa}<K_o<16.3\ \text{GPa}$, and $11.0<K_o'<12.1$. The calculated pressure derivative is somewhat higher than the Yoo and Cynn set, consistent with the stiffer overall isotherm predicted from the simulations. Bulk moduli obtained from the elastic tensor, via Eq. (7), and from volume fluctuations of the simulation cell, Eq. (8), agree to within 0.1 GPa (thus, only a single value is shown). Values obtained in this way should represent the ''true'' initial bulk modulus, since they sample microscopic fluctuations at 1 atm. This is borne out by the fits to the isotherm. Moreover, fitting forms that emphasize the low-pressure regions of the equation of state [i.e., Eq. (5)] yield values of the bulk modulus in closer agreement to the fluctuation-based values than does the Birch–Murnaghan fit using Eq. (4) directly. That this trend is not upheld in the simulation data of Sorescu *et al.*[14] probably arises because they did not include low-pressure states in their study. (Their main objective was to validate their potential against the isotherm of Olinger *et al.*,[6] so no low-pressure simulations were performed.)

TABLE III. Elastic coefficients and isotropic shear modulus (G) for HMX polymorphs.[a]

	β Expt.[b]	β	α	δ[c]
C_{11}	**20.8**	22.2±0.3	30.6±0.5	14.5±0.7($C_{11}=C_{22}$)
C_{22}	26.9	23.9±0.5	23.3±0.8	14.0±0.8($C_{22}=C_{11}$)
C_{33}	**18.5**	23.4±0.5	31.4±0.2	18.0±0.9
C_{44}	4.2	9.2±0.2	0.80±0.04	4.4±0.2($C_{44}=C_{55}$)
C_{55}	**6.1**	11.1±0.1	3.3±0.1	4.4±0.2($C_{55}=C_{44}$)
C_{66}	2.5	10.1±0.1	3.3±0.2	2.3±0.4($C_{66}=C_{11}-C_{12}$)
C_{12}	4.8	9.6±0.7	5.7±0.7	10.3±0.5
C_{13}	12.5	13.2±0.3	13.8±0.7	10.6±0.7($C_{13}=C_{23}$)
C_{23}	5.8	13.0±0.2	6.0±0.3	10.3±0.4($C_{23}=C_{13}$)
C_{15}	**−0.5**	−0.1±0.3		
C_{25}	−1.9	4.7±0.2		
C_{35}	**1.9**	1.6±0.2		
C_{46}	2.9	2.5±0.3		
G		7.0	2.4	2.9

[a]In GPa. For α-HMX, a, b, and c are directed along the $\hat{\mathbf{x}}$, $\hat{\mathbf{y}}$, and $\hat{\mathbf{z}}$ axes, respectively, in a right-handed Cartesian frame. For β-HMX, a is directed along $\hat{\mathbf{x}}$, b is along $\hat{\mathbf{y}}$, and c is in the $\hat{\mathbf{x}}\hat{\mathbf{z}}$ plane. For δ-HMX, a is directed along $\hat{\mathbf{x}}$, b is in the $\hat{\mathbf{x}}\hat{\mathbf{y}}$ plane, and c is along the $\hat{\mathbf{z}}$ axis.

[b]Well-determined experimental values (see text) are in bold. Zaug (Ref. 8) chose a different orientation in his experiments on β-HMX; we have transformed the elastic tensor presented in his study to coincide with the choice made in the present work.

[c]Symmetry-dictated equivalencies of the elastic coefficients for δ-HMX (hexagonal crystal lattice) are indicated.

D. β-HMX elastic tensor

The calculated isothermal elastic tensor for β-HMX is compared in Table III to the one reported by Zaug,[8] corresponding to isentropic conditions (orientation specified in footnote a of the table). Uncertainties in the calculated elastic coefficients represent one standard deviation in values predicted from five contiguous two nanosecond simulation sequences from the overall ten nanosecond simulation. Formal expectations, corresponding to perfect experimental alignment for the chosen crystal orientation, are that nine of the thirteen elastic coefficients would be sampled in Zaug's experiment; see Appendix C. In practice, however, his measurements determined uniquely five of the thirteen elastic constants. These coefficients—C_{11}, C_{33}, C_{55}, C_{15}, and C_{35}—are indicated in bold in the experimental column, and the comparison between the two sets is most meaningful for those particular C_{ij}. Acceptable agreement (percent difference of $\approx 20\%$ or less) is obtained for C_{11}, C_{33}, and C_{35}. The agreement is less good for C_{55}, where the experimental

value is only 55% the calculated one. Similar discrepancies are seen for some of the elements of the elastic tensor that were not determined uniquely in the experiment.

As noted earlier, values of the bulk modulus obtained from the elastic tensor are consistent with those obtained directly from an analysis of volume fluctuations, and these define lower limits to the values extracted from our calculated isotherms, which include significant low-pressure information.

E. Results for α- and δ-HMX

There are no experimental determinations or previous theoretical predictions of the isotherms or elastic tensors for α- and δ-HMX. Starting from the experimental crystal structure for α-HMX,[4] we observed a phase transition between 0.2 and 0.5 GPa characterized by sharp changes in the lattice parameters. In light of this, we restrict the equation of state fits for α-HMX discussed below to pressures less than 0.2 GPa (four pressures). While there was no apparent discontinuity in the δ-HMX isotherm, examination of the individual lattice parameters indicated a gradual, symmetry-class preserving shift that occurs between 1.0 and 2.4 GPa. For this reason, and in analogy with restricting our fits of the Yoo and Cynn[7] data to pressures below 12 GPa, we restrict our fits for δ-HMX to 1.0 GPa and below (six pressures). Pressure-induced phase changes are common in organic crystals, and have been identified for the high explosives β-HMX[7] and hexahydro-1,3,5-trinitro-1,3,5-triazine (RDX).[6,39] This is unsurprising, since anisotropy leads to significant shear strains even under hydrostatic loading.

Values of the bulk modulus extracted from the α- and δ-HMX isotherms, with fits restricted to the intervals specified above, are included in Table II. As for β-HMX, the bulk moduli extracted from the α- and δ-HMX isotherms are consistent with values derived from the elastic tensor and analysis of volume fluctuations. There is an approximately linear correlation between bulk modulus and crystal density, with $K_{o\beta} > K_{o\alpha} (\approx 0.93\, K_{o\beta}) > K_{o\delta} (\approx 0.78\, K_{o\beta})$. This stands in contrast to the quantum chemistry-based predictions of Lewis *et al.*,[15] who obtained zero Kelvin values $K_{o\beta} = 10.2-12.5$ GPa, $K_{o\alpha} = 38.6$ GPa, and $K_{o\delta} = 48.0$ GPa from a fit of the cold curve to $K = V^{-1} d^2E/dV^2$, where V is the specific volume and E is potential energy. Lewis *et al.* cautioned that their predictions should only be regarded as rough estimates due to geometric constraints on crystal lattice parameters imposed in their study, which would be expected in general to lead to overestimates of the bulk moduli. The values reported in the present work should be much more reliable.

Room temperature elastic tensors for α- and δ-HMX are given in Table III. There are no previous reports concerning the elastic coefficients for those polymorphs. The results indicate considerable anisotropy in the diagonal elements of the tensor for α-HMX ($C_{11} \approx C_{33} \sim 1.3 C_{22}$; $C_{55} \approx C_{66} \sim 5 C_{44}$), in contrast to the case of β-HMX where strong anisotropy is not observed. This difference presumably arises due to the qualitatively different molecular packings in the two polymorphs and, insofar as anisotropies in the elastic tensor may have analogs in plastic deformation mechanisms, may have ramifications for the energetics of slip systems in the two materials. This is an issue with practical importance, since differences in mechanical slip systems within a given crystal polymorph have been considered in attempts to explain orientational dependencies of shock response and detonation thresholds in PETN[40] and nitromethane.[41] For δ-HMX, which is of hexagonal symmetry, formal symmetry-based relations exist among the elements of the elastic tensor. These are indicated in Table III, and expectations are fulfilled with the exception of C_{66}, for which the predicted value 2.3 GPa differs by -1.6 GPa from the expected value.

Isotropic shear moduli calculated using Eq. (7) for all three HMX polymorphs are included at the bottom of Table III. Interestingly, the predicted shear moduli for α- and δ-HMX are significantly smaller, by more than a factor of 2, than the value for β-HMX. In a forthcoming conference proceeding, Tappan *et al.*[42] report resonant ultrasound measurements of the longitudinal and transverse sound speeds in pressed samples of HMX (*not* single crystal). The longitudinal and shear wave sound speeds, c_l and c_s, respectively, are related to the bulk and shear moduli via $K = c_l^2 \rho$ and $G = c_s^2 \rho$. The value Tappan *et al.*[42] obtained for the bulk modulus of β-HMX at room temperature, 3.7 GPa under a constant load of 5.6 MPa, is significantly smaller than any reported value for a single crystal. This is not surprising since their pressed sample had a porosity of about 4.4%, and sound speeds are highly sensitive to porosity. It is interesting, however, that they observed a significant decrease in the apparent bulk and shear moduli upon transformation from β- to δ-HMX at $\sim 185\,^{\circ}$C. This is consistent with the present results, and may be of interest with respect to understanding the increased shock sensitivity of δ-HMX relative to β-HMX.

V. CONCLUSIONS

We have used a high level quantum chemistry-based intra- and intermolecular force field to predict the isotherms, isothermal elastic coefficients, and derived isotropic moduli of the three pure polymorphs of HMX at atmospheric pressure and 295 K. Equation of state fitting forms employed in the two previous experimental studies of the β-HMX isotherm were applied to the simulation data. The predicted elastic coefficients and derived bulk moduli for β-HMX are in reasonable agreement with the available experimental data. Based on this work and a preceding analysis due to Menikoff and Sewell,[31] we think that the best value for the ambient isothermal bulk modulus of β-HMX should be increased by ~ 3 GPa to 15–16 GPa. There are no comparable data available for comparison for α- and δ-HMX, and thus the present results comprise the only published information concerning the elastic coefficients and single crystal isotropic moduli for those polymorphs. An interesting observation is that the calculated shear moduli for α- and δ-HMX are significantly smaller than for β-HMX ($\approx 2.5-3$ GPa versus 7 GPa). Bulk moduli calculated from analyses of volume fluctuations are consistent with those extracted directly from the elastic tensor, and these are in acceptable agreement with values extracted from equation of state fitting forms. How-

ever, extracting the initial bulk modulus from an equation of state is highly sensitive to the fitting form chosen, to the method used to perform the fit, and to the interval of data considered. In order to obtain a reliable initial bulk modulus from the isotherm for organic crystals such as HMX, it is necessary to have high-precision information corresponding to pressures below about 1 GPa in order to resolve the rapid change in compressibility at low levels of compression. Of the fitting forms and weighting schemes considered, we found that the third-order Birch–Murnaghan equation of state, fit with a weighting scheme that emphasizes low-pressure data, consistently yields initial moduli in closest agreement with values obtained from microscopic fluctuations which correspond to the true thermodynamic parameter.

ACKNOWLEDGMENTS

T.D.S and R.M. are supported by the Los Alamos ASCI High Explosives Effort. D.B. and G.D.S. are funded by the University of Utah Center for the Simulation of Accidental Fires and Explosions (C-SAFE), funded by the Department of Energy, Lawrence Livermore National Laboratory, under subcontract No. B341493.

APPENDIX A: ISOTHERMAL AND ISENTROPIC ELASTIC TENSORS

For a crystal the isothermal and isentropic elastic tensors can be related through the use of thermodynamic identities.[43] The result is

$$\bar{\bar{C}}_S=\bar{\bar{C}}_T+\frac{V_o T}{c_\varepsilon}(\bar{\bar{C}}_T:\overline{\beta})\otimes(\bar{\bar{C}}_T:\overline{\beta}), \tag{A1}$$

where $\bar{\bar{C}}_S$ and $\bar{\bar{C}}_T$ are the fourth rank isentropic and isothermal elastic tensors, respectively, $\overline{\beta}$ is the second rank thermal strain tensor, and c_ε is the specific heat at constant strain. The thermal strain tensor can be obtained from x-ray diffraction determination of the crystal lattice parameters as a function of temperature. The strain tensor is defined in terms of the second rank transformation tensor from fractional (crystallographic) to Cartesian coordinates $\overline{\mathbf{h}}$ by

$$\overline{\varepsilon}=\tfrac{1}{2}[(\overline{\mathbf{h}_\mathbf{0}^\mathbf{T}})^{-1}\overline{\mathbf{h}^\mathbf{T}}\overline{\mathbf{h}}\mathbf{h}_\mathbf{0}^{-1}-\mathbf{1}], \tag{A2}$$

and the thermal strain tensor is

$$\overline{\beta}=\left(\frac{\partial\overline{\varepsilon}}{\partial T}\right)_{\text{stress}}. \tag{A3}$$

For a monoclinic crystal, such as β-HMX,

$$\overline{\mathbf{h}}=\begin{pmatrix} a & 0 & c\cos\beta \\ 0 & b & 0 \\ 0 & 0 & c\sin\beta \end{pmatrix}, \tag{A4}$$

where a, b, and c are lattice lengths and β is the monoclinic angle. The columns of $\overline{\mathbf{h}}$ are the Cartesian lattice vectors $\boldsymbol{a}$, $\boldsymbol{b}$, and $\boldsymbol{c}$.

For HMX the temperature derivatives of the lattice parameters have been measured,[44] and are as follows: -0.29×10^{-5}/K, 11.60×10^{-5}/K, and 2.30×10^{-5}/K for a, b, and c, respectively; and 2.58×10^{-5}/K for β.

We note that the fluid dynamic analog for the bulk modulus is

$$K_S=K_T+\frac{VT}{c_v}(\beta K_T)^2, \tag{A5}$$

where c_v is the specific heat at constant volume and, in this case, β is the volumetric coefficient of thermal expansion. Substituting the isotropic average values for HMX, one find that K_S is 5% greater than K_T. This affects the isotropic sound speeds by roughly 2%.

APPENDIX B: RELATIONSHIP BETWEEN COMPLIANCE AND ELASTIC TENSOR IN THE PRESENT WORK

The stiffness and compliance tensors relate tensoral stress $\overline{\boldsymbol{\sigma}}$ and strain $\overline{\boldsymbol{\varepsilon}}$ via

$$\overline{\sigma}_{ij}=\bar{\bar{C}}_{ijkl}:\overline{\varepsilon}_{kl} \quad\text{and}\quad \overline{\varepsilon}_{ij}=\bar{\bar{S}}_{ijkl}:\overline{\sigma}_{kl}. \tag{B1}$$

In this case, the fundamental relation between the stiffness tensor $\bar{\bar{\mathbf{C}}}$ and compliance tensor $\bar{\bar{\mathbf{S}}}$ is

$$\bar{\bar{S}}_{ijkl}\bar{\bar{C}}_{klmn}=\tfrac{1}{2}(\delta_{im}\delta_{jn}+\delta_{in}\delta_{jm}). \tag{B2}$$

Since the stress and strain are symmetric tensors, we can express them using Voigt notation ($x_{11}\equiv x_1$, $x_{22}\equiv x_2$, $x_{33}\equiv x_3$, $x_{23}=x_{32}\equiv x_4$, $x_{13}=x_{31}\equiv x_5$, $x_{12}=x_{21}\equiv x_6$), and define $\bar{\bar{C}}_{ij,kl}\equiv\overline{C}_{V(a),V(b)}$, where $V(a)$ and $V(b)$ denote the Voigt indices, e.g., $11\rightarrow1$ or $23=32\rightarrow4$, etc. This allows us to write $\boldsymbol{\sigma}_i=\overline{C}_{ij}\boldsymbol{\varepsilon}_l$ and $\boldsymbol{\varepsilon}_i=\overline{S}_{ij}\boldsymbol{\sigma}_l$, which is the common way of presenting the elastic coefficients (i.e., as symmetric 6×6 matrices). It does not follow in general, however, that $\overline{\mathbf{S}}$ and $\overline{\mathbf{C}}$ in second-rank form are related through simple matrix inversion, due to ambiguity in how one defines the contracted stress and strain. That is, $\bar{\bar{C}}_{ij,kl}\equiv\overline{C}_{V(a),V(b)}$ does not imply that $\bar{\bar{S}}_{ij,kl}=\overline{S}_{V(a),V(b)}$.

Following Tsai,[34] we defined

$$\boldsymbol{\varepsilon}=(\varepsilon_{11},\varepsilon_{22},\varepsilon_{33},2\varepsilon_{23},2\varepsilon_{13},2\varepsilon_{12})^T,$$
$$\boldsymbol{\sigma}=(\sigma_{11},\sigma_{22},\sigma_{33},\sigma_{23},\sigma_{13},\sigma_{12})^T, \tag{B3}$$

for which

$$\bar{\bar{S}}_{ij,kl}=\overline{S}_{V(a),V(b)},\ \text{for}\ V(a)\ \text{and}\ V(b)=1,2,\ \text{or}\ 3;$$
$$2\bar{\bar{S}}_{ij,kl}=\overline{S}_{V(a),V(b)},\ \text{for}\ V(a)=1,2,\ \text{or}\ 3\ \text{and}\ V(b)=4,5,\ \text{or}\ 6\ (\text{and vice versa});$$
$$4\bar{\bar{S}}_{ij,kl}=\overline{S}_{V(a),V(b)},\ \text{for}\ V(a)\ \text{and}\ V(b)=4,5,\ \text{or}\ 6;\ \text{and}$$
$$\bar{\bar{C}}_{ij,kl}=\overline{C}_{V(a),V(b)}\ \text{for all combinations of}\ V(a)\ \text{and}\ V(b). \tag{B4}$$

With this choice, the second-rank stiffness and compliance are in fact simple matrix inverses of one another.

APPENDIX C: SOUND SPEEDS AND ELASTIC TENSOR: ANALYSIS OF ZAUG'S EXPERIMENT (REF. 8)

The sound speeds are determined by the acoustic tensor,

$$\bar{\bar{\mathbf{A}}}^{ipjp} = \bar{\bar{\mathbf{C}}}^{ipjp} + \delta^{ij}\overline{\sigma}^{pq}. \tag{C1}$$

For a wave propagating in the $\hat{\mathbf{n}}$ direction, if one defines the matrix

$$\overline{\mathbf{b}}(\hat{\mathbf{n}})^{ij} = n_p \bar{\bar{\mathbf{A}}}^{ipjp} n_q, \tag{C2}$$

then the sound speeds are the solution to the equation

$$\det(\overline{\mathbf{b}}(\hat{\mathbf{n}})^{ij} - \rho c^2 \delta_{ij}) = 0; \tag{C3}$$

or, in terms of the stiffness tensor,

$$\det[\overline{\mathbf{c}}(\hat{\mathbf{n}})^{ij} - (\rho c^2 - \overline{\sigma}_{nn})\delta_{ij}] = 0, \tag{C4}$$

where

$$\overline{\mathbf{c}}(\hat{\mathbf{n}})^{ij} = n_p \bar{\bar{C}}^{ipjp} n_q. \tag{C5}$$

At ambient conditions the stress $\overline{\sigma}_{nn}$ is small compared to the modulus, $K_0 = \rho c^2$, and can be neglected. For a monoclinic crystal only 13 of the components of the stiffness tensor are nonzero. In terms of Voigt indices for the stiffness tensor, the sound speeds of a monoclinic crystal are the eigenvalues of the matrix $\overline{b}(\hat{n})$ with components,

$$\begin{aligned}
\overline{\mathbf{b}}_{11} &= n_1^2 C_{11} + n_2^2 C_{66} + n_3^2 C_{55} + 2n_1 n_3 C_{15}, \\
\overline{\mathbf{b}}_{22} &= n_1^2 C_{66} + n_2^2 C_{22} + n_3^2 C_{44} + 2n_1 n_3 C_{46}, \\
\overline{\mathbf{b}}_{33} &= n_1^2 C_{55} + n_2^2 C_{44} + n_3^2 C_{33} + 2n_1 n_3 C_{35}, \\
\overline{\mathbf{b}}_{12} &= \overline{\mathbf{b}}_{21} = n_2 n_3 (C_{46} + C_{25}) + n_1 n_2 (C_{12} + C_{66}), \\
\overline{\mathbf{b}}_{13} &= \overline{\mathbf{b}}_{31} = n_1^2 C_{15} + n_2^2 C_{46} + n_3^2 C_{35} + n_1 n_3 (C_{13} + C_{55}), \\
\overline{\mathbf{b}}_{23} &= \overline{\mathbf{b}}_{32} = n_2 n_3 (C_{44} + C_{23}) + n_1 n_2 (C_{25} + C_{46}).
\end{aligned} \tag{C6}$$

The ISLS measurements of Zaug[8] for β-HMX are for acoustic waves propagating in the plane normal to the (0,1,0) face. With $\hat{n} = (\cos\theta, 0, \sin\theta)$, the matrix reduces to

$$\begin{aligned}
\overline{\mathbf{b}}_{11} &= \cos^2(\theta) C_{11} + \sin^2(\theta) C_{55} + \sin(2\theta) C_{15}, \\
\overline{\mathbf{b}}_{22} &= \cos^2(\theta) C_{66} + \sin^2(\theta) C_{44} + \sin(2\theta) C_{46}, \\
\overline{\mathbf{b}}_{33} &= \cos^2(\theta) C_{55} + \sin^2(\theta) C_{33} + \sin(2\theta) C_{35}, \\
\overline{\mathbf{b}}_{12} &= \overline{\mathbf{b}}_{21} = 0, \\
\overline{\mathbf{b}}_{13} &= \overline{\mathbf{b}}_{31} = \cos^2(\theta) C_{15} + \sin^2(\theta) C_{35} + \tfrac{1}{2}\sin(2\theta)(C_{13} + C_{55}), \\
\overline{\mathbf{b}}_{23} &= \overline{\mathbf{b}}_{32} = 0.
\end{aligned} \tag{C7}$$

We note that in this plane, b depends formally on nine of the thirteen independent components for the stiffness tensor with monoclinic symmetry: C_{11}, C_{33}, C_{44}, C_{55}, C_{66}, C_{13}, C_{15}, C_{35}, and C_{46}. To determine the four other components (C_{12}, C_{22}, C_{23}, and C_{25}), measurements of the sound speed in another plane would be needed. Empirically, the measured sound speeds are only sensitive to five of the nine elastic tensor elements identified above.

[1] T.R. Gibbs and A. Popolato, *LASL Explosive Property Data* (University of California, Berkeley, 1980); B.M. Dobratz, "LLNL Explosives Handbook: Properties of Chemical Explosives and Explosive Simulants," Report No. UCRL-52997, 16 March, 1981.
[2] C.S. Choi and H.P. Boutin, Acta Crystallogr., Sect. B: Struct. Crystallogr. Cryst. Chem. **26**, 1235 (1970).
[3] Y. Kohno, K. Maekawa, N. Azuma, T. Tsuchioka, T. Hashizume, and A. Imamura, Kogyo Kayako **53**, 227 (1992).
[4] H.H. Cady, A.C. Larson, and D.T. Cromer, Acta Crystallogr. **16**, 617 (1963). Note that the "*y*" fractional coordinate for atom N_1 in Table II should have a negative sign.
[5] R.E. Cobbledick and R.W.H. Small, Acta Crystallogr., Sect. B: Struct. Crystallogr. Cryst. Chem. **30**, 1918 (1974).
[6] B. Olinger, B. Roof, and H. Cady, in *Proceedings of the Symposium (International) on High Dynamic Pressures* (C.E.A., Paris, 1978), pp. 3–8.
[7] C.-S. Yoo and H. Cynn, J. Chem. Phys. **111**, 10229 (1999).
[8] J.M. Zaug, in *Proceedings of the Eleventh Detonation Symposium*, 1998, p. 498.
[9] R. Menikoff and T.D. Sewell, Combust. Theory Modell. **6**, 103 (2002).
[10] For example, M.R. Baer, Thermochim. Acta **38**, 351 (2002).
[11] A.V. Dzyabchenko, T.S. Pivina, and E.A. Arnautova, J. Mol. Struct. **67**, 378 (1996).
[12] T.D. Sewell, J. Appl. Phys. **83**, 4142 (1998).
[13] D.C. Sorescu, B.M. Rice, and D.L. Thompson, J. Phys. Chem. B **102**, 6692 (1998).
[14] D.C. Sorescu, B.M. Rice, and D.L. Thompson, J. Phys. Chem. B **103**, 6783 (1999).
[15] J.P. Lewis, T.D. Sewell, R.B. Evans, and G.A. Voth, J. Phys. Chem. B **104**, 1009 (2000).
[16] D. Bedrov, G.D. Smith, and T.D. Sewell, J. Chem. Phys. **112**, 7203 (2000).
[17] D. Bedrov, G.D. Smith, and T.D. Sewell, Chem. Phys. Lett. **324**, 64 (2000).
[18] D. Bedrov, A. Chakravarthy, G.D. Smith, T.D. Sewell, R. Menikoff, and J.M. Zaug, J. Comput.-Aided Mater. Des. **8**, 77 (2001).
[19] D. Bedrov, G.D. Smith, and T.D. Sewell, in *Proceedings of the 2001 American Physical Society Topical Conference on Shock Compression in Condensed Matter*, June 24–29, 2001, Atlanta, GA, edited by M.D. Furnish, N.N. Thadani, and Y. Horie, p. 403.
[20] In Ref. 19, p. 399.
[21] D.C. Sorescu, B.M. Rice, and D.L. Thompson, J. Phys. Chem. A **102**, 8386 (1998).
[22] G.D. Smith and R.K. Bharadwaj, J. Phys. Chem. B **103**, 3570 (1999).
[23] M. Parrinello and A. Rahman, J. Chem. Phys. **76**, 2662 (1982).
[24] M.P. Allen and D.J. Tildesley, *Computer Simulation of Liquids* (Oxford University Press, Oxford, 1987).
[25] L.D. Landau and E.M. Lifschitz, *Theory of Elasticity* (Pergammon, Oxford, 1970), Subsection 10.
[26] M. Parrinello and A. Rahman, J. Appl. Phys. **52**, 7182 (1981).
[27] G.J. Martyna, M.E. Tuckerman, D.J. Tobias, and M.L. Klein, Mol. Phys. **87**, 1117 (1996).
[28] For example, W.W. Wood, in *Physics of Simple Fluids*, edited by H.N.V. Temperley, J.S. Rowlinson, and G.S. Rushbrooke (North-Holland, Amsterdam, 1968), Chap. 5, p. 115.
[29] W. Fickett and W.C. Davis, *Detonations* (University of California, Berkeley, 1979).
[30] J.-P. Poirier, *Introduction to the Physics of the Earth's Interior* (Cambridge University Press, Cambridge, 1999), p. 64.
[31] R. Menikoff and T.D. Sewell, High Press. Res. **21**, 121 (2001).
[32] Menikoff and Sewell (Ref. 31) performed the fit to Eq. (4) in the $p-V$ plane by writing $p(V) = af_1(V) + bf_2(V)$ and minimizing the residual $R = \Sigma(\Delta P)^2 = \Sigma[P_i - af_1(V_i) - bf_2(V_i)]^2$ with respect to a and b, where $a = K_o$ and $b = K_o K_o'$.
[33] C.-S. Yoo, H. Cynn, W.M. Howard, and N. Holmes, in *Proceedings of the Eleventh International Detonation Symposium*, August 31–September 4, 1998, Snowmass Village, CO, edited by J. M. Short, p. 951. The sections

of this Proceedings article dealing with HMX are expanded upon in Ref. 7.
[34] S.W. Tsai, *Mechanics of Composite Materials, Part II, Theoretical Aspects*, AFML Technical Report No. AFML-TR-66-149, November, 1966.
[35] B. Olinger, P.M. Halleck, and H.H. Cady, J. Chem. Phys. **62**, 4480 (1975).
[36] Following Menikoff and Sewell (Ref. 31), we ignore the Yoo and Cynn (Ref. 7) data point at 0.20 GPa, since it leads to the aphysical prediction of a nonmonotonic U_s-U_p curve.
[37] *LASL Shock Hugoniot Data*, edited by S. P. Marsh (University of California Press, Berkeley, 1980).
[38] D.C. Sorescu (private communication).
[39] B.J. Baer, J. Oxley, and M. Nicol, High Press. Res. **2**, 99 (1990).
[40] J.J. Dick and J.P. Ritchie, J. Phys. IV **4**, 393 (1994).
[41] J.J. Dick, J. Phys. Chem. **97**, 6193 (1993).
[42] A.S. Tappan, A.M. Renlund, J.C. Stachowiak, J.C. Miller, and M.S. Oliver, ''Mechanical properties determination by real-time ultrasonic characterization of thermally damaged energetic materials,'' in Proceedings of the 12th International Detonation Symposium, August 11–16, 2002, San Diego, CA (to be published), presently available at: http://www.sainc.com/onr/detsymp/PaperSubmit/FinalManuscript/pdf/Tappan-134.pdf
[43] D.C. Wallace, *Thermodynamics of Crystals* (Dover, New York 1998), Chap. 1, Sec. 2.
[44] M. Herrmann, Engel, and Eisenreich Z. Kristallogr. **204**, 121 (1993).